Journal of Nondestructive Evaluation (2021) 40:70
https://doi.org/10.1007/s10921-021-00800-x

Evaluation of the Residual Plastic Deformation in Low-Carbon Steel with the Oscillatory Rotating Eddy Current Method

Nan Wang[1] · Xiucheng Liu[1] · Jieming Yang[1] · Cunfu He[1]

Received: 15 September 2020 / Accepted: 21 July 2021 / Published online: 9 August 2021

Abstract
Residual plastic deformation induced in low-carbon steels usually demonstrates anisotropy. Eddy current method is applicable for the residual plastic deformation evaluation. However, it is difficult to efficiently evaluate both the principal strain direction and magnitude of residual plastic deformation with the conventional eddy current method. To solve these limitations, a novel method of oscillatory rotating eddy current (OREC) was developed and successfully applied in characterizing the anisotropy of residual plastic deformation in low-carbon steels. The parameters of eddy current response obtained under different frequencies were extracted to characterize the plastic deformation and then the characterization performances of extracted parameters were compared. The compound voltage signal and real part of the impedance could better characterize the residual plastic deformation than the imaginary part of the impedance. It was found that the angle of the major axis of the selected 8-shaped patterns measured with OREC was a good indicator of the principal strain direction. As the residual plastic deformation was increased, the length of the major axis of the 8-shaped patterns monotonously increased despite its sensitivity to the plastic deformation was frequency-dependent.

Keywords Oscillatory rotating eddy current · Residual plastic deformation · Anisotropy evaluation · Low-carbon steel

1 Introduction

Plastic forming technology is an effective tool for manufacturing steel parts with desired geometrical or irregular shapes. It employs externally applied fields of force and temperature to cause plastic deformations accompanied by the refinement of the microstructure and mechanical properties of a material [1]. The evaluation results of the residual plastic deformation in specific regions can be used in the forming process adjustment and product quality control. Plastic deformation may induce the redistribution of residual stress, dislocations and micro-defects inside the ferromagnetic material. As a result, both the conductivity and permeability of the material are changed during the plastic deformation process. Thus, the electromagnetic properties of the ferromagnetic material are related to the degree of plastic deformation. Accordingly, nondestructive testing (NDT) methods, such as measurements of magnetic hysteresis loop [2, 3], magnetic Barkhausen noise [4, 5], leakage magnetic flux [6] and eddy current [7], have been developed for evaluating the residual plastic strain through measuring the electromagnetic properties of ferromagnetic materials.

Among available electromagnetic NDT tools, eddy current testing is rapid and convenient for in-line system integration. The theoretical basis and successful applications of eddy current in the evaluation of the plastic strain in ferromagnetic materials have been reported [8–12] to highlight the significant dependency of the eddy current responses on the plastic strain. However, most of the experiments were carried out in the default case that the principal direction of plastic deformation was already known or the generated unidirectional eddy current field was parallel to the principal direction of plastic deformation.

The residual plastic strain is usually inhomogeneous or uneven in different directions, so it is necessary to develop eddy current testing technologies for evaluating the principal strain direction and magnitude of residual plastic deformation. Eddy current measurement in multiple directions can be realized by manually or mechanically rotating a unidirectional probe [13]. However, it is time-consuming and the lift-off variation accompanied by the probe rotation may cause a

✉ Xiucheng Liu
xiuchliu@bjut.edu.cn

[1] Faculty of Materials and Manufacturing, Beijing University of Technology, Beijing, People's Republic of China

large uncertainty and even error in measurement results. To solve the problem in the unidirectional eddy current method, the vector superposition principle of electromagnetic fields can be employed to automatically generate the rotating eddy current field in the tested materials. It is feasible to employ two orthogonally overlapped unidirectional planar coils, which are fed with single-frequency continuous waves of 90° out of phase, in order to produce rotating eddy current (REC) [14–16].

In our previous study, we discussed the drawbacks of the REC in crack orientation detection and emphasized that the REC method could only be applied in the rough quantification of crack orientation and might even fail to detect the cracks with specific orientations in ferromagnetic materials. By introducing amplitude-modulated excitation currents into the REC test, a novel method of oscillatory rotating eddy current (OREC) was developed [17], it can achieve the high angular resolution of the crack orientation determination in both non-ferromagnetic and ferromagnetic materials. In OREC method, the period of the low-frequency modulation signal determined the spatial rotation speed of the OREC field and the envelop profiles of the high-frequency carrier signals were plotted in a polar diagram to demonstrate the anisotropy in electromagnetic properties of the tested specimen.

With the OREC method, in this study, the residual plastic deformation in low-carbon steel was evaluated based on the 8-shaped polar diagrams of compound voltage signal and real and imaginary parts of the impedance. We found that the angle and the length of the major axis of the 8-shaped curve were good indicators of the principal strain direction and the residual plastic strain, respectively. In addition, the performances of the OREC method under different feature parameters and frequencies were experimentally compared.

The remainder of the paper is organized as follows. The operation principle and experimental set-up for OREC method are briefly introduced in Sect. 2. The sample preparation and typical results are given in Sect. 3. The results are discussed in Sect. 4 and conclusions are drawn in Sect. 5.

2 Operation Principle and Experimental Set-Up

When two orthogonal rectangular excitation coils (marked excitation coil X and excitation coil Y, respectively) were placed above the surface of a ferromagnetic material (Fig. 1a), the eddy current field with a certain magnitude and orientation could be generated by carefully controlling the currents flowing in two coils according to the vector superposition principle of eddy current fields.

To generate OREC field in the ferromagnetic material, stepping-modulated excitation currents in phase were synchronously fed into the two excitation coils. The waveforms of the stepping-modulated sinusoidal currents of I_{x_k} and I_{y_k} are plotted in Fig. 1c. The two-channel excitation currents at each step are expressed as follows:

$$\begin{aligned} I_{x\_k}(k,t) &= i_0 \sin\left(\alpha_k\right) \sin\left(2\pi f_c t\right) \\ I_{y\_k}(k,t) &= i_0 \cos\left(\alpha_k\right) \sin\left(2\pi f_c t\right) \end{aligned} \tag{1}$$

where $\alpha_k = 2\pi k/N$ ($k = 0, 1, 2, 3 \ldots N$) and i_0 is the maximum amplitude of the current. The functions of $\sin(\alpha_k)$ and $\cos(\alpha_k)$ follow the stepped envelop of low frequency. Thus, the envelop of the low frequency (f_m) modulated signal is discretized into N steps. At each step, the amplitude and the orientation of the compound eddy current field with high frequency (f_c) are directly determined by the values of $\sin(\alpha_k)$ and $\cos(\alpha_k)$.

I_{x_k} and I_{y_k} respectively represent the eddy current fields along X and Y directions, so the compound eddy currents

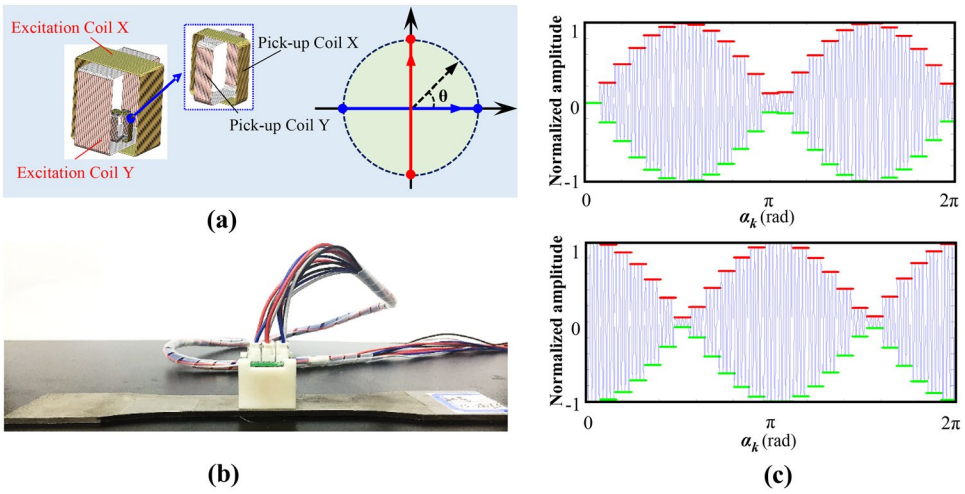

Fig. 1 **a** Structural configuration and **b** picture of the eddy current sensor. **c** Typical waveform diagram of the stepping-modulated currents fed into the two orthogonal excitation coils

flowing in the tested material have an amplitude of $I_{co}(k)$ and an angle of $\theta_{co}(k)$ against X-axis:

$$\begin{aligned} I_{\mathrm{co}}(k) &= i_0\sqrt{I_{x\_k}(k,t)^2 + I_{y\_k}(k,t)^2} = i_0 \sin 2\pi f_c t \\ \theta_{co}(k) &= \arctan\left(I_{x\_k}/I_{y\_k}\right) = \alpha_k \end{aligned} \tag{2}$$

As indicated in Eq. (2), the compound eddy current field demonstrates a linear increasing rotation angle and a time-varying amplitude. The OREC fields can be considered as step-rotated eddy current field and the step of the rotation angle is fixed as $2\pi/N$. In eddy current testing, the available detection area, which is covered by a circumference centered on the position of the eddy current sensor, is evenly divided into N sections. In each segmental area with a specific orientation angle of α_k, the eddy current field oscillates for several periods and the number of oscillation periods, M, can be estimated as $M = 1/(f_{\mathrm{m}}N)$. During the OREC detection process, the recorded eddy current responses can be demodulated into a sequence of N elements, which can be used to evaluate the electromagnetic properties of the material under different orientation angles of α_k.

The eddy current sensor used in this study was equipped with the coils demonstrated in Fig. 1a. The parameters of the excitation coils and pick-up coils were identical to those of the sensor used in the previous study [17]. The entire sensor was encased by a 3D printed plastic bracket and placed in the center of the tensile test specimen (Fig. 1b). To automatically generate the step-rotated eddy current field and detect the eddy current responses in two orthogonal directions, an experimental set-up was constructed based on an industrial personal computer and PCI-based functional cards. A dual-channel arbitrary waveform generation card PCI6968 was used to output the stepping-modulated sinusoidal currents for the two channels of excitation coils. The two-channel excitation signals together with the output voltage signals of U_{x_k}(t) and U_{y_k}(t) respectively induced in the pick-up coil X and pick-up coil Y were acquired by a four-channel acquisition card PCI8504.

The operation of the whole system was regulated by LabVIEW and MATLAB programs in the host computer. The orientation of the excitation coil X of the eddy current sensor was parallel to the specimen tension direction. An increment of 3.75° in the rotation angle of α_k was selected and a total of 96 times of unidirectional eddy current testing was performed per modulation period. For the unidirectional eddy current testing with a certain orientation angle of α_k, the compound voltage signal (A_{c_k}), real and imaginary parts of the compound impedance were extracted as feature parameters. The compound voltage, A_{c_k}, is estimated as

$$A_{c\_k} = \sqrt{A_{x\_k}^2 + A_{y\_k}^2} \tag{3}$$

where A_{x_k} and A_{y_k} are the peak voltages of the U_{x_k}(t) and U_{y_k}(t), respectively. Fast Fourier transform tool was employed to transform the signal of U_{x_k}(t) and corresponding excitation signal into the vectors of $\mathbf{Z}_{\mathrm{ux}\_k}$ and $\mathbf{Z}_{ix\_k}$, respectively. The impedance of the eddy current response received by the pick-up coil X, $\mathbf{Z}_{x\_k}$, was estimated by dividing the vector $\mathbf{Z}_{\mathrm{ux}\_k}$ by the vector $\mathbf{Z}_{ix\_k}$. The similar operation was performed with the eddy current response received by the pick-up coil Y for calculating the impedance of $\mathbf{Z}_{y\_k}$. The compound impedance of $\mathbf{Z}_{co\_k}$ is the summation of $\mathbf{Z}_{x\_k}$ and $\mathbf{Z}_{y\_k}$. The real and imaginary parts of the compound impedance is referred as Re($\mathbf{Z}_{co\_k}$) and Im($\mathbf{Z}_{co\_k}$).

3 Sample Preparation and Experimental Results

Low-carbon steel sheets with a thickness of 3 mm were used for sample preparation. The chemical composition of the used low-carbon steel is listed in Table 1. Twenty one dog-bone tensile specimens with identical sizes were cut from the steel sheet with the wire cutting technique. The sizes of tensile specimen are illustrated in Fig. 2a.

Preliminary tensile test was conducted with one of the specimens and the yield strength of low carbon steel was evaluated to be around 196 MPa. Another specimen without tension was used as the reference. The uniaxial tension load beyond the estimated yield strength of 196 MPa was applied on the remaining nineteen specimens to force them directly into the plastic stage and then removed. Through changing the position of the starting point (with maximum tensile stress) for unloading, the residual plastic deformation of different degrees was induced in the specimens. The measured residual plastic strain of the twenty specimens ranged from zero to about 13.28% (Fig. 2b).

OREC tests were alternatively performed with the twenty specimens to measure the angular-dependent feature parameters of eddy current. The tested frequencies of the high-frequency carrier currents included $f_c = 5$ kHz, 10 kHz and 50 kHz and corresponding modulated frequency was $f_{\mathrm{m}} = 100$ Hz. Taking the results obtained at the carrier frequency of 5 kHz as an example, the procedure for plotting the polar diagrams of feature parameters was interpreted. The results of the feature

Table 1 Chemical composition of low-carbon steel sheets

Composition	C	S	Si	Mn	P	Al	Cu	Cr
Wt%	0.041	0.0082	0.017	0.11	0.012	0.028	0.012	0.014

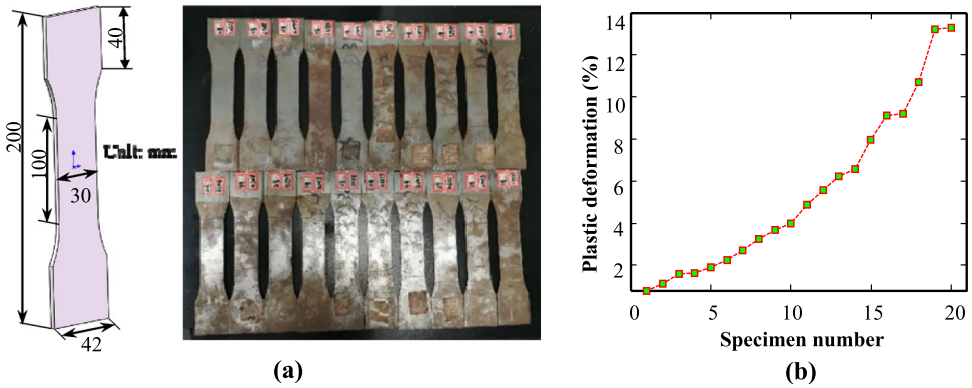

Fig. 2 **a** Sizes and picture of the specimens and **b** measured results of residual plastic strain for all the tested specimens

parameters of A_{c_k}, Re($\mathbf{Z}_{co\_k}$) and Im($\mathbf{Z}_{co\_k}$) obtained from all the tested specimens are shown in Fig. 3a–c, respectively.

The results of angular-dependent feature parameters were subtracted from the reference curve to highlight the dependency of residual curves of feature parameters on the residual plastic strain. The residuals of A_{c_k} and Re($\mathbf{Z}_{co\_k}$) experienced the sinusoidal fluctuation with the change in the tested angle and the residual curves shifted upward with the increase in the residual plastic strain (Fig. 3a, b). The results in Fig. 3c showed the opposite trend and the compound voltage profiles gradually shifted downward as the residual plastic strain increased.

The results in Fig. 3a–c could be redrawn in polar diagrams to indicate the anisotropy of feature parameters of the eddy current in the tested specimen. A sliding average algorithm was compiled in MATLAB software to smooth the residual curves shown in Fig. 3. When the step of the sliding window was selected as 5 data points, the smoothed residual curves of A_{c_k}, Re(Z_{co_k}) and Im(Z_{co_k}) demonstrated 8-shaped trajectories (Fig. 4). Figure 5 shows the results of the three feature parameters measured under different carrier frequencies.

4 Discussion

The results in Fig. 5 indicate that the OREC method could be used to measure the anisotropy of eddy current response in the tested material in a fast speed. The tension direction of the specimens was orientated along the transverse axis (0°–180°) of the polar diagram. Therefore, it was believed that the principal directions of the residual plastic deformation were parallel to the transverse axis or vertical axis (90°–270°).

The 8-shaped trajectories of the A_{c_k} and Re($\mathbf{Z}_{co\_k}$) had similar orientations. Their major and minor axes were respectively close to the transverse and vertical axes of the polar diagram, indicating that the 8-shaped trajectories of A_{c_k} and Re($\mathbf{Z}_{co\_k}$) were the good pattern for the determination of principal strain directions. The orientation angle of the major (or minor) axis against the transverse axis is defined as the estimated principal strain direction. The principal directions of the residual plastic deformation estimated with the 8-shaped patterns in Fig. 5 are shown in Fig. 6.

For the 8-shaped patterns of A_{c_k} and Re(Z_{co_k}), the principal strain directions represented by the major or minor axis remained nearly unchanged under different carrier frequencies. It was found that there was a small angle of around 8°–15° between the tension direction and the major axis of the 8-shaped trajectories. In our previous study, the equivalent systematic error was evaluated to be 10.8° [17]. The small systematic error was caused by the imperfect coil installation because the relative angle error between the two pairs of excitation coils and pick-up coils might cause minor mismatch between the marked and actual zero angle directions.

In the results of A_{c_k} and Re(Z_{co_k}), the pattern of the imaginary part of the impedance demonstrated complicated dependences on the plastic strain and carrier frequency. For instance, when the carrier frequency of the OREC excitation signal was about 5 kHz, the orientation of the pattern of Im(Z_{co_k}) was close to that of Re(Z_{co_k}) in the range of low plastic strain and then rotated around 90° in the range of the large plastic strain higher than 1.5% (Fig. 5c). 8-shaped patterns superposed with strong noise were observed in the case with a carrier frequency of 10 kHz (Fig. 5f). When the carrier frequency was 50 kHz, the patterns of the Im(Z_{co_k}) were basically the same under the conditions of different plastic strains and had 8-shaped trajectories (Fig. 5i). The imaginary part of the impedance mainly reflected the information of magnetic permeability, which strongly relied on both the plastic strain and magnetization frequency [18]. The anisotropy of magnetic permeability is mainly determined by the orientation of hard or easy magnetization axis of the material. For the material with residual plastic deformation, its easy magnetization axis is affected by unpredicted factors such as

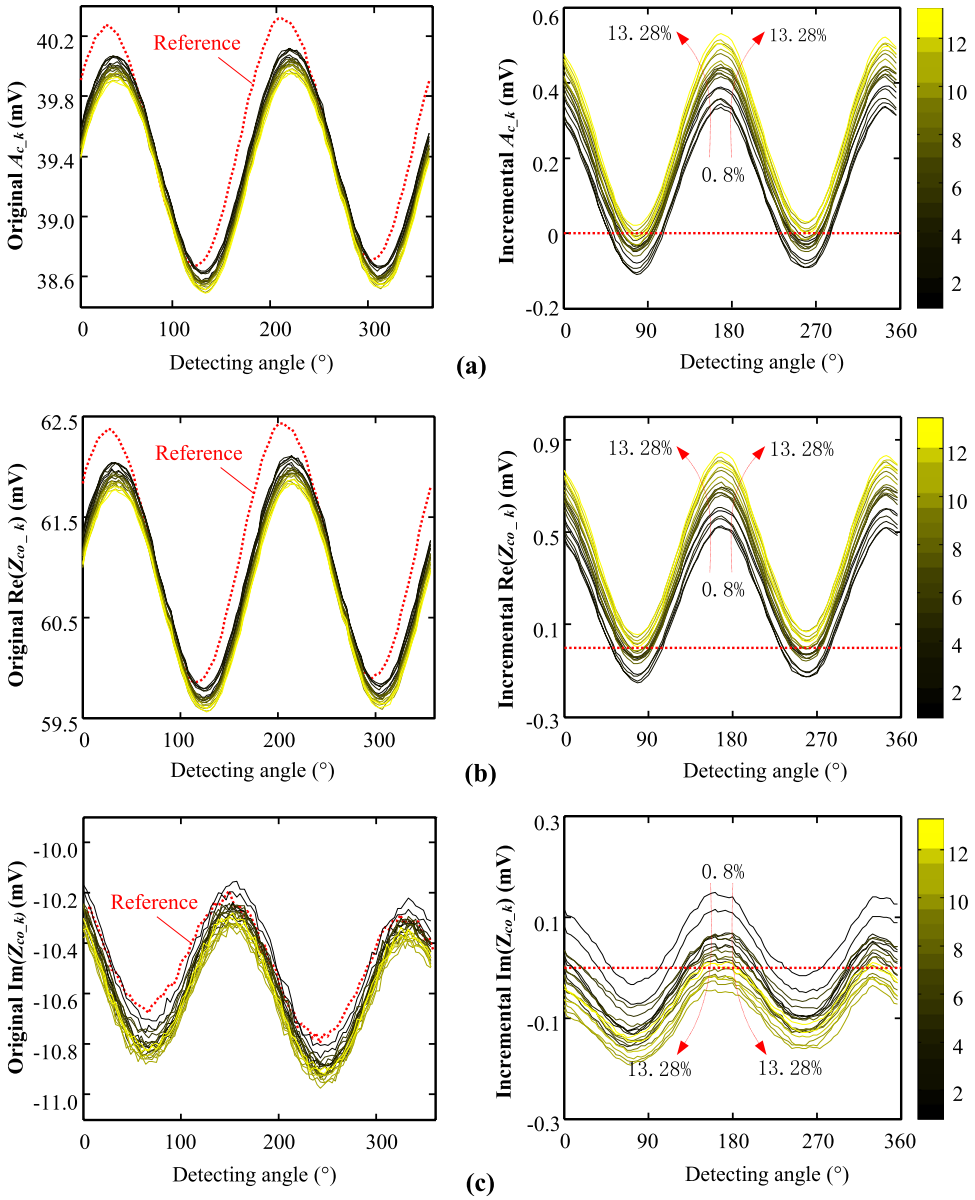

Fig. 3 Results of the feature parameters of **a** A_{c_k}, **b** Re(Z_{co_k}) and **c** Im(Z_{co_k}). The charts in the left column show the original data and the charts in the right column demonstrate the smoothed results of the increment of the feature parameters caused by the residual plastic strain

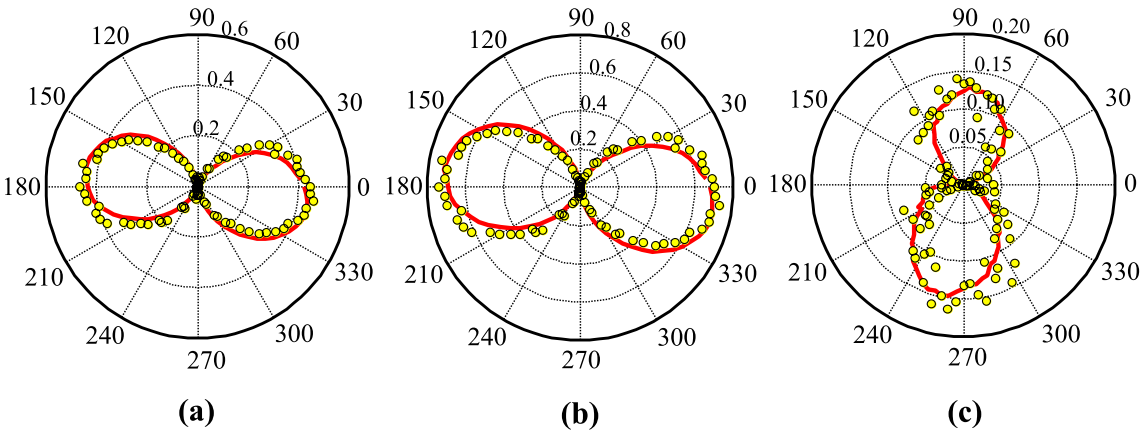

Fig. 4 Polar diagrams of the parameters of **a** A_{c_k}, **b** Re(Z_{co_k}) and **c** Im(Z_{co_k}) measured from the specimen with a residual plastic strain of 6.2%. The circles indicate the measured data points and the solid lines indicate the results obtained after data smoothing operation

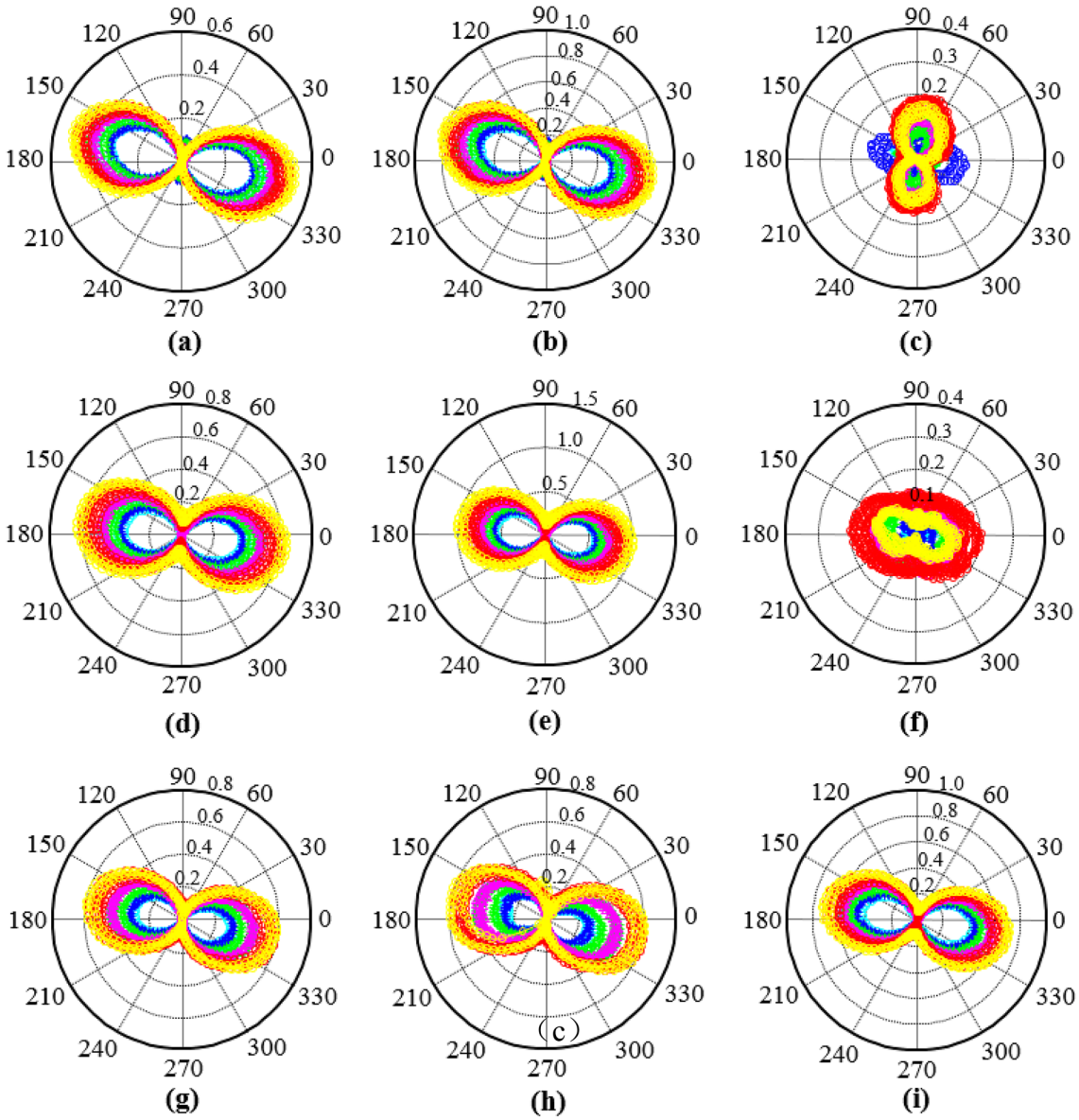

Fig. 5 Polar diagrams of the three feature parameters measured under different carrier frequencies. 8-shaped patterns of test results characterized by the parameters of A_{c_k} were obtained when the carrier frequency are **a** 5 kHz, **d** 10 kHz and **g** 50 kHz; results characterized by the parameters of $\mathrm{Re}(Z_{co\_k})$ were obtained when the carrier frequency are **b** 5 kHz, **e** 10 kHz and **h** 50 kHz; and test results characterized by the parameters of $\mathrm{Im}(Z_{co\_k})$ were obtained when the carrier frequency are **c** 5 kHz, **f** 10 kHz and **i** 50 kHz

the distribution of dislocation, the orientation of grains and the residual stress state. Therefore, the accurate relationship between the anisotropy of magnetic permeability and the residual plastic strain field is still unpredictable. The huge differences in the results as sketched in the right column diagrams indicated that the careful selection of carrier frequency used in OREC method was important for estimating the principal direction of residual plastic strain. Here, only the patterns of the $\mathrm{Im}(Z_{co\_k})$ measured in the case of $f_c = 50$ kHz were used for the determination of the principal strain direction and the achieved accuracy was comparable to that of the feature parameter of $\mathrm{Re}(Z_{co\_k})$.

In the tensile test experiments, only the actual residual plastic strain along the tension direction was measured. Accordingly, the semi-major axis, which was represented by the mean value of the feature parameters at the two endpoints of the major axis, was estimated to characterize the residual plastic strain. Figure 7a–c demonstrate the dependencies of the semi-major axis on the residual plastic strain. The solid symbols represent the experimentally measured

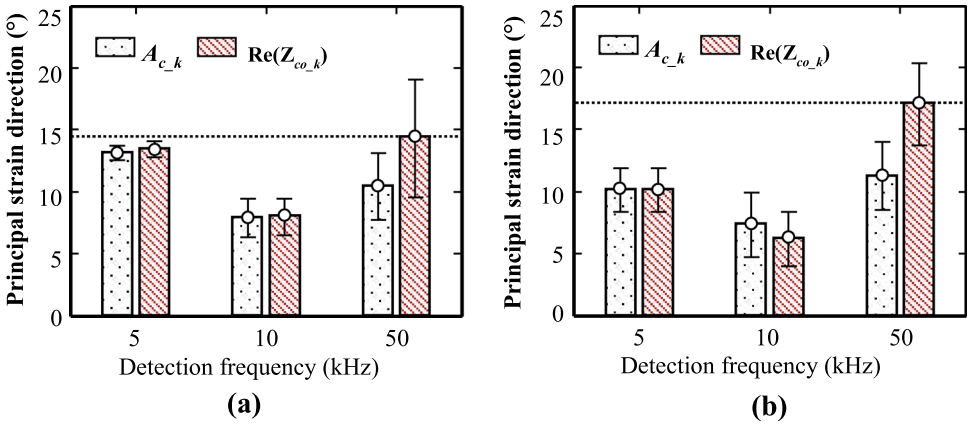

Fig. 6 Principal directions of the residual plastic deformation estimated with the 8-shaped pattern of residual A_{c_k} and Re(Z_{co_k}). **a** transverse and **b** vertical principal directions

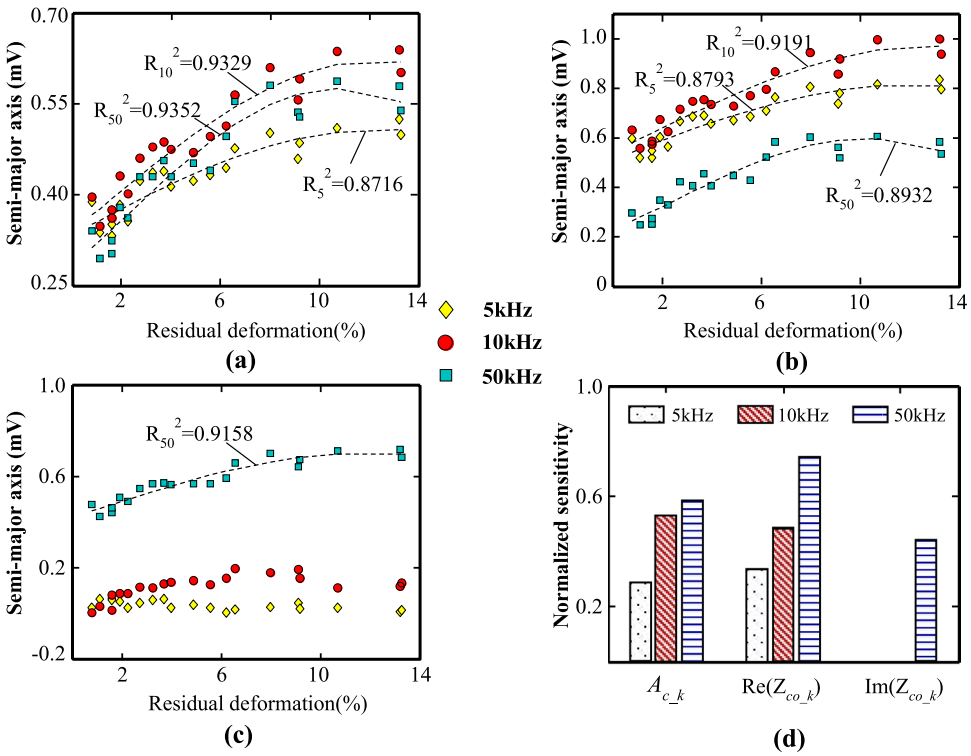

Fig. 7 Dependency of semi-major axis of the 8-shaped patterns on the residual plastic strain. **a–c** Results of the feature parameters of A_{c_k}, Re(Z_{co_k}) and Im(Z_{co_k}). **d** Frequency-dependent sensitivity of the semi-major axis to the residual plastic strain

data and the dotted lines are fitting curves obtained with exponential-type equation.

The values of R-square of the fitted equations for all the cases were higher than 0.85. Therefore, with the increase in the residual plastic strain, the values of the semi-major axis for three feature parameters investigated in this study displayed an exponential uptrend except Im(Z_{co_k}) measured under $fc = 5$ kHz and 10 kHz. Among the investigated cases, the semi-major axis extracted from the A_{c_k} pattern at the frequency of $f_c = 50$ kHz had the highest accuracy in the residual plastic strain evaluation with a R-square of 0.9352 and a RMSE value of 1.73%.

When the plastic strain increased from 0.8 to 13.28%, the relative growth rate of the semi-major axis was calculated to roughly estimate the sensitivity of the semi-major axis to plastic strain. The estimated sensitivities of three feature parameters at different carrier frequencies are shown in Fig. 7d. Obviously, the sensitivity of semi-major axis to the variation of residual plastic strain was frequency-dependent. As stated in the Ref. [18], the permeability decreases due to the increment of plastic deformation occurred in the carbon steel. For a given excitation frequency, the reduction in permeability of the steel leads to an increase in the penetration depth of the eddy current field. However, the intensity of the eddy current-induced secondary magnetic field at the surface decreases. This causes a drop in the response voltage of the measured coil. As a results, the sensitivity of the OREC method on the variation of the permeability (or the

plastic deformation) reduces. By increasing the operation frequency, the intensity of the eddy current-induced secondary magnetic field at the surface can be improved. Then the voltage output by the measured coil can be increased to improve the sensitivity of the OREC method on the variation of the permeability (or the plastic deformation). In the study, a frequency of 50 kHz was more sensitive to the residual plastic strain in the evaluation as compared with 5 kHz and 10 kHz.

5 Conclusions

In this paper, a new stepping-modulated excitation method for rotating eddy current was developed and the proposed OREC method was used to evaluate the residual plastic deformation in low-carbon steel. The experimental results proved the high efficiency of OREC method in measuring the anisotropy of eddy current response. The 8-shaped patterns of the selected parameters of eddy current were good indicators for the anisotropy of residual strain. The measurement speed and fineness of the 8-shaped patterns could be adjusted by tuning the carrier and modulation frequencies of the excitation current. The compound voltage signal and the real part of the impedance demonstrated the better performance in characterizing the residual plastic deformation than the imaginary part of the impedance. The determination of the principal strain direction and the quantitative evaluation of residual plastic strain can be realized respectively by estimating the angle and the length of the major axis of the selected 8-shaped patterns.

Acknowledgements This study was supported by the National Key R&D Program of China (2018YFF01012300), National Natural Science Foundation of China (Project No. 11872081) and Beijing Nova Program of Science and Technology (Grant No. Z191100001119044).

References

1. Li, J., Xu, M., Leng, J., et al.: Modeling plastic deformation effect on magnetization in ferromagnetic materials. J. Appl. Phys. **111**(6), 1–4 (2012)
2. Kwun, H., Burkhardt, G.L.: Effects of grain size, hardness, and stress on the magnetic hysteresis loops of ferromagnetic steels. J. Appl. Phys. **61**(4), 1576–1579 (1987)
3. Vertesy, G., Meszaros, I., Tomas, I., et al.: Nondestructive indication of plastic deformation of cold-rolled stainless steel by magnetic minor hysteresis loops measurement. J. Magn. Magn. Mater. **285**(3), 335–342 (2005)
4. Chavez-Gonzalez, A.F., Perez-Benitez, J.A.: A model for the influence of plastic deformation on magnetic Barkhausen noise in carbon steel. Mater. Res. Express **6**(10), 1–14 (2019)
5. Neslusan, M., Trsko, L., Minarik, P., et al.: Non-destructive evaluation of steel surfaces after severe plastic deformation via the Barkhausen noise technique. Metals **8**(12), 1–15 (2018)
6. Kuroda, M., Yamanaka, S., Yamada, K., et al.: Evaluation of residual stresses and plastic deformations for iron-based materials by leakage magnetic flux sensors. J. Alloy Compd. **314**(1–2), 232–239 (2001)
7. Gorkunov, E.S., Savrai, R.A., Makarov, A.V., et al.: Application of an Eddy-current method for the assessment of stored plastic deformation and residual mechanical properties after cyclic loading of an annealed medium-carbon steel. Russ. J. Nondestr. Test. **43**(4), 228–233 (2007)
8. Meng, F., Liu, X., Wang, H., et al.: Characterization of elastic and plastic behaviors in steel plate based on eddy current technique using a portable impedance analyzer. J. Sens. **2017**, 1–12 (2017)
9. Gonchar, A.V., Bizyaeva, O.N., Klyushnikov, V.A., et al.: Ultrasonic and eddy-current study of plastic deformation in austenitic-steel welds. Russ. J. Nondestr. Test. **52**(10), 610–616 (2016)
10. Bai, P., Shi, P., Zhao, Y., et al.: Joint effect of residual stress and plastic deformation on pulsed eddy current response signals in 304 austenitic stainless steel. Int. J. Appl. Electromagn. Mech. **63**(1), 19–30 (2020)
11. Matsumoto, T., Uchimoto, T., Takagi, T., et al.: Investigation of electromagnetic nondestructive evaluation of residual strain in low carbon steels using the eddy current magnetic signature (EC-MS) method. J. Magn. Magn. Mater. **479**, 212–221 (2019)
12. Xie, S., Chen, Z., Chen, H., et al.: Evaluation of plastic deformation and characterization of electromagnetic properties using pulsed eddy current testing method. Int. J. Appl. Electromagn. Mech. **45**(1–4), 755–761 (2014)
13. Lei, N., Udpa, L., Udpa, S., et al.: Rotating field eddy current (RoFEC)-probe for steam generator inspection. Int. J. Appl. Electromagn. Mech. **33**(3), 1279–1285 (2010)
14. Koyama, K., Hoshikawa, H.: Basic study of a new ECT probe using uniform rotating direction eddy current. Rev. Prog. Quant. Nondestr. Eval. **16**, 1067–1074 (1997)
15. Hamia, R., Cordier, C., Dolabdjian, C.: Eddy-current non-destructive testing system for the determination of crack orientation. NDT E Int. **61**, 24–28 (2014)
16. Yang, G., Dib, G., Udpa, L., et al.: Rotating field EC-GMR sensor for crack detection at fastener site in layered structures. IEEE Sens. J. **15**(1), 463–470 (2015)
17. Liu, X., Yang, J., Wu, B., et al.: A novel generation method of oscillatory rotating eddy current for crack orientation determination and detection in metal plates. NDT E Int. **97**, 1–10 (2018)
18. Cai, W., Chen, H., Xie, S., et al.: A study on influence of plastic deformation on the global conductivity and permeability of carbon steel. Int. J. Appl. Electromagn. Mech. **45**, 371–378 (2014)